Magnetic properties and specific heat studies of RE_2Pd_2Cd (RE = La,Ce,Nd)

2006 J. Phys.: Condens. Matter 18 5473

(http://iopscience.iop.org/0953-8984/18/23/018)

INSTITUTE OF PHYSICS PUBLISHING JOURNAL OF PHYSICS: CONDENSED MATTER

J. Phys.: Condens. Matter **18** (2006) 5473–5492 doi:10.1088/0953-8984/18/23/018

Magnetic properties and specific heat studies of RE_2Pd_2Cd (RE = La, Ce, Nd)

Sudhindra Rayaprol, Ahmet Doğan and Rainer Pöttgen

Institut für Anorganische und Analytische Chemie, Westfälische Wilhelms-Universität Münster, Corrensstraße 30, 48149, Münster, Germany

E-mail: pottgen@uni-muenster.de

Received 27 February 2006, in final form 29 March 2006
Published 26 May 2006
Online at stacks.iop.org/JPhysCM/18/5473

Abstract

The intermetallic compounds RE_2Pd_2Cd (RE = La, Ce, Nd) were prepared from the elements in sealed tantalum tubes in a water-cooled sample chamber of an induction furnace. The structure of Nd_2Pd_2Cd was refined on the basis of x-ray single crystal data: $P4/mbm$, $a = 774.15(9)$, $c = 386.73(7)$ pm, $wR2 = 0.0321$, 214 F^2 values, 12 variables. The compounds of this series exhibit interesting magnetic behaviour, namely complex magnetism in Ce_2Pd_2Cd and ferromagnetism in Nd_2Pd_2Cd ($T_C = 23.7$ K). La_2Pd_2Cd is a Pauli paramagnet. We have carried out detailed investigations of the magnetic and heat capacity behaviour of La_2Pd_2Cd, Ce_2Pd_2Cd and Nd_2Pd_2Cd.

1. Introduction

The family of ternary intermetallics of the type R_2T_2X (R = actinoid or rare earth metal, T = transition metal and X = In, Sn, Mg) have been extensively studied over the last 15 years for their interesting crystal chemistry and physical properties ([1], and references therein). The magnetic properties of the uranium and cerium containing R_2T_2X (hence forth called 221) intermetallics exhibit interesting phenomena, such as non-magnetic ground states, Kondo behaviour, heavy fermions or spin-fluctuating systems. In these compounds the physical properties are strongly influenced by the chemical bonding among the constituent elements. Most of these 221 intermetallics crystallize in the Mo_2FeB_2 type, a ternary ordered version of the U_3Si_2 structure [1, 2]. The structural and magnetic properties of 221 indides and stannides have been widely studied over the years (for a review on the structure property relations see [1]).

With palladium as the transition metal component, the series of M_2Pd_2In indides crystallizing with the Mo_2FeB_2 structure has been synthesized and studied for their structural, magnetic and thermodynamic properties [3, 4]. The effect of non-stoichiometry on the magnetic properties of the $Ce_2(Pd_{1-x}Ni_x)_2In$ solid solution has also been studied [5, 6] and physical properties of the whole series of cerium based indides, Ce_2T_2In (T = Ni, Cu, Rh, Pd, Pt and Au) have been reported [7, 8]. Apart from the indides, interesting studies on some plumbides have also been published recently [9–11].

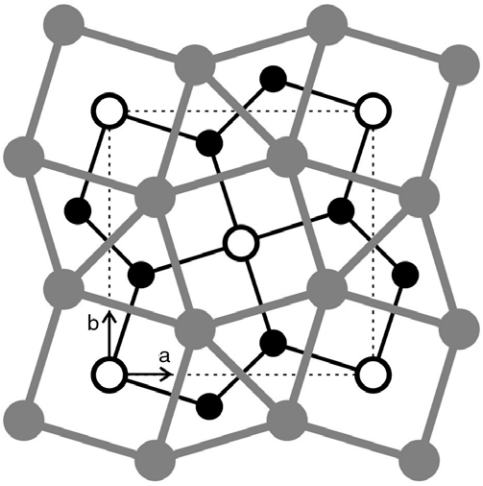

Figure 1. Projection of the Nd_2Pd_2Cd structure onto the xy plane. Neodymium, palladium, and cadmium atoms are drawn as medium grey, filled, and open circles, respectively. All atoms lie on mirror planes at $z = 0$ (thin lines) and $z = 1/2$ (thick lines). The two-dimensional $[Pd_2Cd]$ network and the distorted AlB_2 and CsCl related slabs are emphasized.

However, only a few reports exist on the cadmium containing 221 intermetallics [12–17]. We have observed interesting magnetic properties in Ce_2T_2Cd intermetallics. For example, $Ce_2Ni_{1.88}Cd$ and $Ce_2Rh_{1.86}Cd$ are intermediate-valent cerium compounds [12, 13], whereas cerium is trivalent in Ce_2Au_2Cd, and the compound is a heavy fermion with antiferromagnetic ordering around 5 K [14, 15]. Gd_2Au_2Cd exhibits coexistence of ferromagnetism and spin-glass anomalies [16]. In a continuation of our investigations on RE_2T_2Cd intermetallics, here we present the magnetic and heat capacity data of RE_2Pd_2Cd for RE = La, Ce, and Nd.

2. Experimental details

2.1. Synthesis

The 221 intermetallics with indium and tin can conveniently be prepared by arc-melting the starting elements. However, owing to the low boiling point of cadmium (1043 K), these samples have to be prepared in closed reaction containers. The starting materials for the preparation of the title compounds were ingots of lanthanum, cerium and neodymium (Johnson-Matthey or Kelpin), palladium powder (about 200 mesh, Degussa-Hüls) and a cadmium rod (Johnson-Matthey), all with stated purities better than 99.9%. The larger ingots of the rare earth metals were first cut into smaller pieces and arc-melted into small buttons under purified argon. The premelting of the rare earth metals reduces shattering during the induction melting. The elements were then weighed in 2:2:1 atomic ratio and sealed in small tantalum tubes under purified argon [18]. The sealed tantalum tubes were then placed in a water-cooled quartz sample chamber of a high frequency furnace (Hüttinger Elektronik, Freiburg, type TIG 1.5/300) under flowing argon [19]. The elements were brought to reaction through inductive annealing at 1670 K for about 1 min, and were subsequently annealed at around 870 K for 2–4 h. The temperature was controlled through a Sensor Therm Methis MS09 pyrometer with an accuracy of ± 30 K. The samples do not react with tantalum and could easily be separated from the container by mechanical fragmentation. The synthesis conditions are similar to those given in [13].

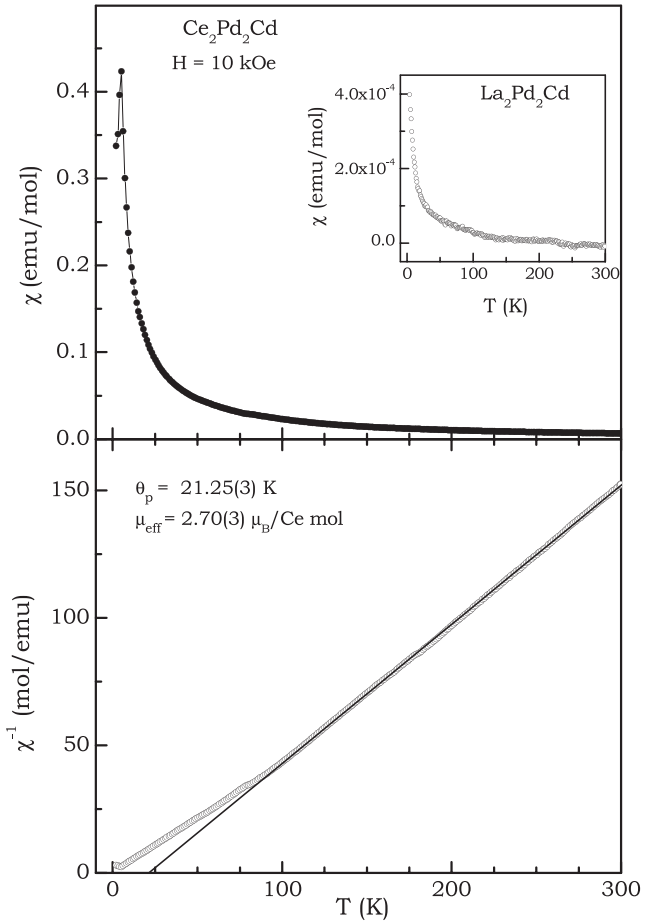

Figure 2. dc $\chi(T)$ for Ce_2Pd_2Cd measured under a field of 10 kOe. The straight line passing through the χ^{-1} curve is the fit from Curie–Weiss law. The inset shows the susceptibility behaviour of La_2Pd_2Cd.

2.2. X-ray imaging plate data and structure refinement

The purity of the samples was checked through Guinier powder patterns using Cu Kα_1 radiation and α-quartz ($a = 491.30$, $c = 540.46$ pm) as an internal standard. The tetragonal lattice parameters were obtained from least-squares refinements of the Guinier powder data. The powder patterns of the three compounds were properly indexed using the atomic positions of Ce_2Pd_2Cd [2] and Nd_2Pd_2Cd for intensity calculations [20]. The refined lattice parameters for La_2Pd_2Cd and Ce_2Pd_2Cd were $a = 784.47(8)$, $c = 398.03(9)$ pm, and $a = 778.3(1)$, $c = 392.9(2)$ pm, respectively (for Nd_2Pd_2Cd see table 1). The data for Ce_2Pd_2Cd are in good agreement with the previously reported data ($a = 777.90(6)$, $c = 393.28(6)$ pm) [2].

Irregularly shaped single crystals of Nd_2Pd_2Cd were isolated from the annealed sample by mechanical fragmentation and examined by Laue photographs on a Buerger precession camera (equipped with an imaging plate system Fujifilm BAS-1800) in order to establish suitability for intensity data collection. Intensity data were collected at room temperature using a four-circle

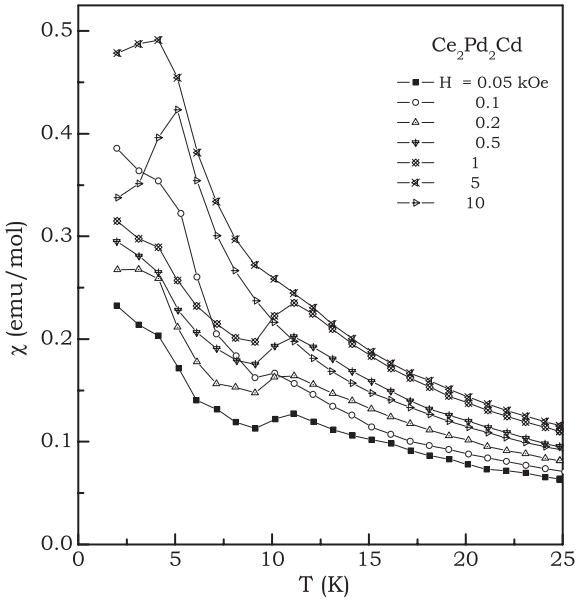

Figure 3. dc $\chi(T)$ for Ce_2Pd_2Cd measured under various applied fields.

Table 1. Crystal data and structure refinement for Nd_2Pd_2Cd.

Empirical formula	Nd_2Pd_2Cd
Structure type	Mo_2FeB_2
Molar mass	613.68 g mol^{-1}
Unit cell dimensions	$a = 774.15(9)$ pm
(Guinier data)	$c = 386.73(7)$ pm
	$V = 0.2318$ nm^3
Space group	$P4/mbm$
Pearson symbol, Z	tP10, 2
Calculated density	8.79 g cm^{-3}
Crystal size	$100 \times 100 \times 180$ μm^3
Transmission ratio (max/min)	1.43
Absorption coefficient	33.9 mm^{-1}
$F(000)$	520
θ range	3°–30°
Range in hkl	$\pm 10, \pm 10, +5$
Total no. reflections	1439
Independent reflections	214 ($R_{\text{int}} = 0.0439$)
Reflections with $I > 2\sigma(I)$	210 ($R_{\text{sigma}} = 0.0184$)
Data/parameters	214/12
Goodness-of-fit on F^2	1.342
Final R indices [$I > 2\sigma(I)$]	$R1 = 0.0189$; $wR2 = 0.0319$
R indices (all data)	$R1 = 0.0199$; $wR2 = 0.0321$
Extinction coefficient	0.0048(2)
Largest diff. peak and hole	1.45 and -1.46 e Å^{-3}

diffractometer (CAD4) with graphite monochromatized Mo Kα radiation (71.073 pm) and a scintillation counter with pulse height discrimination. The scans were performed in the $\omega/2\theta$

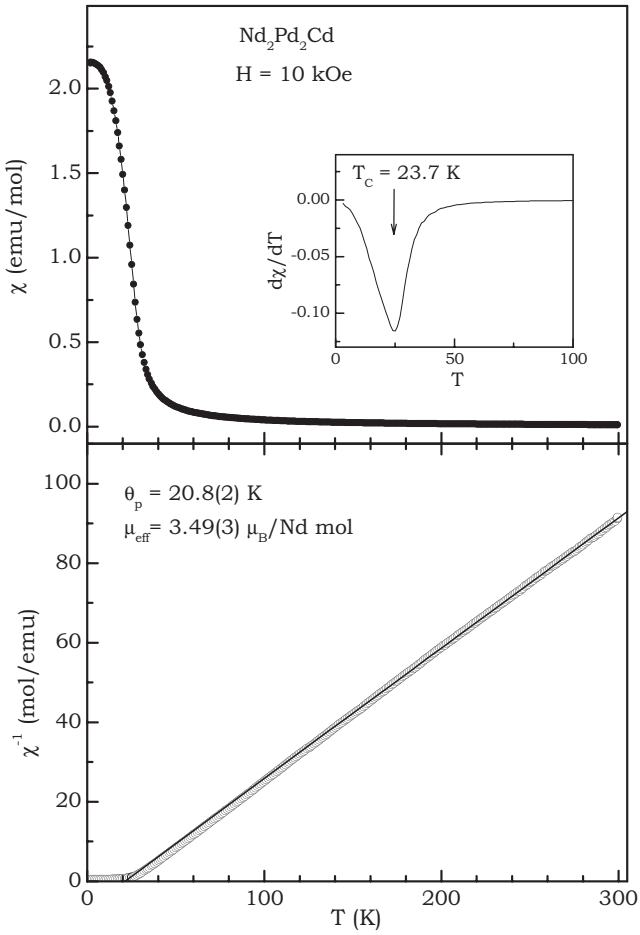

Figure 4. dc $\chi(T)$ for Nd_2Pd_2Cd measured under a field of 10 kOe. The straight line passing through the χ^{-1} curve is the fit from Curie–Weiss law. The inset shows the first derivative of susceptibility to determine the ordering temperature.

mode. An empirical absorption correction was applied on the basis of Ψ-scan data followed by a spherical absorption correction. All relevant crystallographic details are listed in table 1.

The systematic extinctions of the data set were compatible with space group $P4/mbm$, in agreement with the previous investigations on Ce_2Pd_2Cd [2]. The atomic parameters of the cerium compound were taken as starting values and the structure was refined using SHELXL-97 (full-matrix least-squares on F_0^2) [21] with anisotropic atomic displacement parameters for all three sites. As a check for the correct composition, the occupancy parameters were refined in separate series of least-squares cycles. All sites were fully occupied within one standard uncertainty. In the final cycles the ideal occupancies were assumed again. A final difference Fourier synthesis revealed no significant residual peaks (see table 1). The refined positional parameters and interatomic distances are listed in tables 2 and 3. Further details on the structure refinements are available[1].

[1] Details may be obtained from: Fachinformationszentrum Karlsruhe, D-76344 Eggenstein-Leopoldshafen (Germany), by quoting the Registry No. CSD-416292.

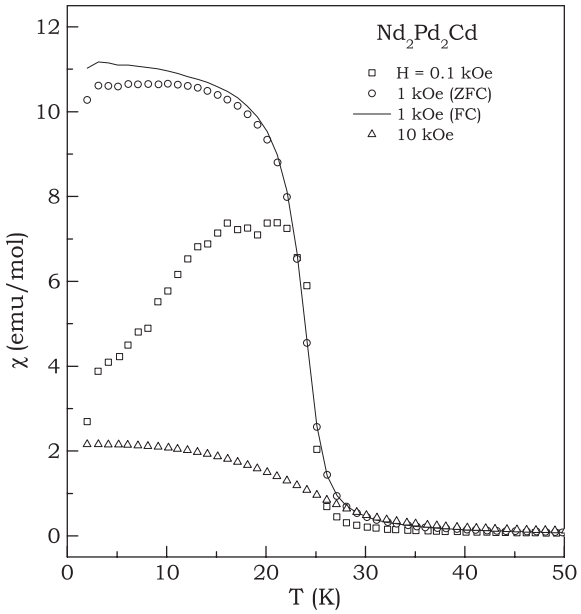

Figure 5. dc $\chi(T)$ for Nd_2Pd_2Cd measured under various applied fields in the zero field state of the sample. The plot also shows field cooled measurement for $H = 1$ kOe.

Table 2. Atomic coordinates and anisotropic displacement parameters (pm^2) for Nd_2Pd_2Cd. The anisotropic displacement factor exponent takes the form: $-2\pi^2[(ha^*)^2U_{11} + \cdots + 2hka^*b^*U_{12}]$. U_{eq} is defined as a third of the trace of the orthogonalized U_{ij} tensor. $U_{13} = U_{23} = 0$.

Atom	Wyck. pos.	x	y	z	$U_{11} = U_{22}$	U_{33}	U_{12}	U_{eq}
Nd	4h	0.173 84(4)	$1/2 + x$	1/2	86(2)	74(2)	−11(1)	82(2)
Pd	4g	0.371 91(6)	$1/2 + x$	0	107(2)	110(3)	−28(2)	108(2)
Cd	2a	0	0	0	103(3)	198(4)	0	135(2)

Table 3. Interatomic distances (pm) in Nd_2Pd_2Cd calculated with the powder lattice parameters. Standard deviations are all equal or smaller than 0.1 pm.

Nd:	2	Pd	290.5	Pd:	1	Pd	280.5
	4	Pd	305.4		2	Nd	290.6
	4	Cd	345.3		2	Cd	304.5
	1	Nd	380.6		4	Nd	305.4
	2	Nd	386.7	Cd:	4	Pd	304.5
	4	Nd	404.6		8	Nd	345.3

2.3. Property measurements

Magnetism and heat capacity of RE_2Pd_2Cd (RE = La, Ce, Nd) were measured on a Quantum Design–Physical Property Measurement System using ACMS and HC options, respectively. The samples were put in gelatin capsules for magnetic measurements, and were mounted on the platform of a pre-calibrated puck using *Apizeon N* grease for the heat capacity measurement.

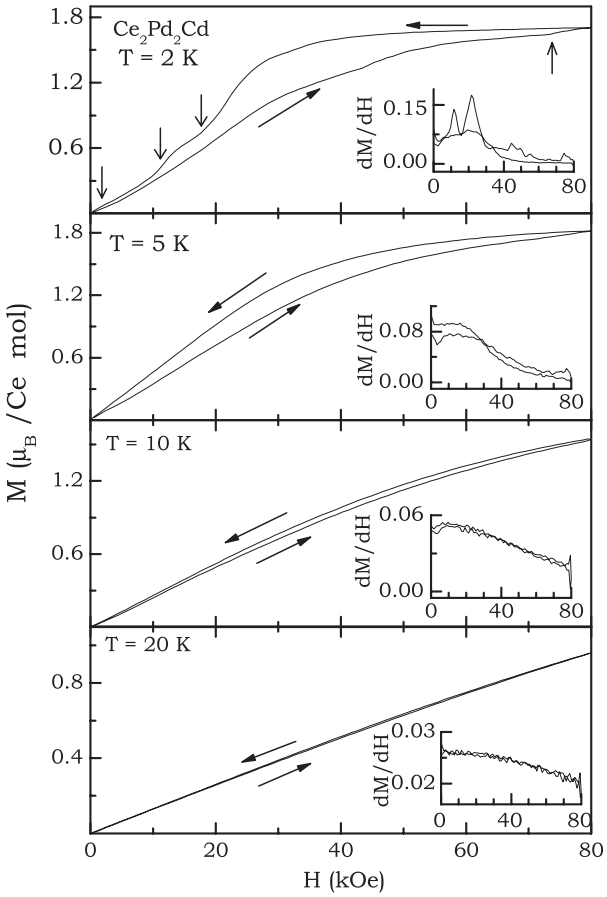

Figure 6. Magnetization as a function of field for Ce_2Pd_2Cd measured at several temperatures. The inset in each panel shows the first derivative of magnetization, plotted to highlight the field induced changes in magnetism.

3. Results and discussions

3.1. Crystal chemistry

La_2Pd_2Cd, Ce_2Pd_2Cd, and Nd_2Pd_2Cd crystallize with the tetragonal Mo_2FeB_2 type structure, space group $P4/mbm$, an ordered version of the U_3Si_2 type. The lanthanum and neodymium compound are reported herein for the first time. A projection of the Nd_2Pd_2Cd structure is presented in figure 1. The structure can be considered as a simple 1:1 intergrowth of AlB_2 and CsCl related slabs of compositions $NdPd_2$ and NdCd. The lattice parameters decrease from the lanthanum to neodymium compound as expected from the lanthonoid contraction. The crystal chemistry of these materials has already been described in detail for the cerium compound. For further information we refer to [2] and to a recent review [1].

3.2. dc susceptibility

In figure 2 we show the dc magnetic susceptibilities of Ce_2Pd_2Cd and La_2Pd_2Cd. Samples were zero field cooled (ZFC) from room temperature to 2 K. The dc susceptibility (χ) for

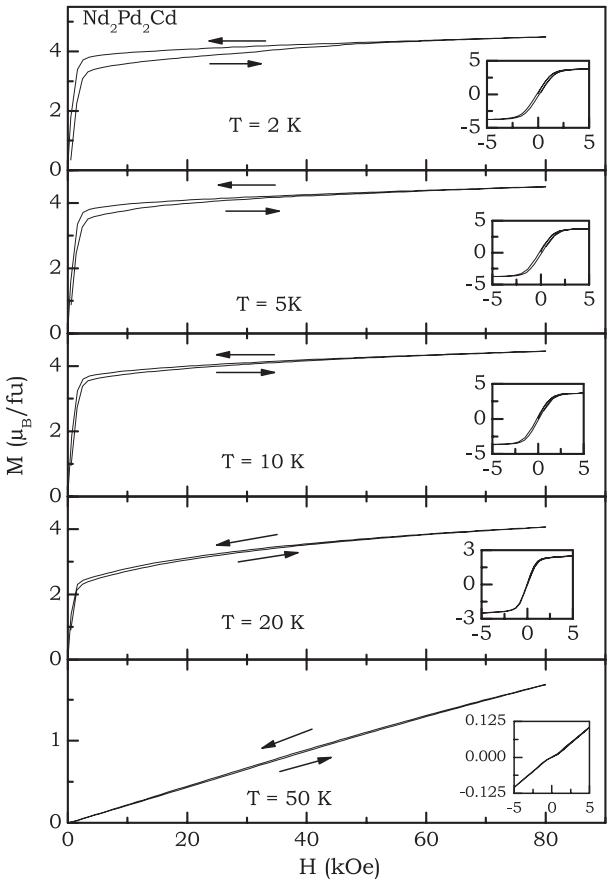

Figure 7. Magnetization as a function of field for Nd_2Pd_2Cd measured at several temperatures. The inset in each panel shows hysteresis loops recorded at these temperatures.

Ce_2Pd_2Cd increases monotonously with decreasing temperature and exhibits a well defined peak around 5 K as if undergoing antiferromagnetic ordering. The inverse susceptibility (χ^{-1}) deviates from the Curie–Weiss law below 100 K owing to crystal-field effects and the onset of magnetic ordering. From the high temperature Curie–Weiss fitting the paramagnetic Curie temperature (θ_p) is 21.2(3) K and the effective Bohr magneton number (μ_{eff}) is 2.70(2) μ_B/Ce mol, which is slightly higher than the expected value of 2.54 μ_B for a free Ce^{3+} ion. The positive value of θ_p establishes ferromagnetic interactions in Ce_2Pd_2Cd at higher temperatures. The large difference in θ_p and T_N indicates inhomogeneous magnetism or short-range magnetic interactions. La_2Pd_2Cd is a typical Pauli paramagnet with a moment value of the order of 4×10^{-4} emu mol^{-1} at the lowest temperature measured. The increase in susceptibility with decreasing temperature is most likely due to traces of paramagnetic impurities.

In order to understand the nature of the magnetic ordering at low temperatures, we have measured susceptibility at various fields in the temperature range of 2–25 K, after cooling in zero field in every case. In figure 3 we show the dc χ measured under $H = 0.05$, 0.1, 0.2, 0.5, 1, 5 and 10 kOe. A small peak around 10 K appears for measurements done with $H \leqslant 1$ kOe. χ increases below 10 K with another peak around 5 K. For $H < 5$ kOe, we observe ordering around two temperatures, 5 and 10 K. It may be recalled here that the binary

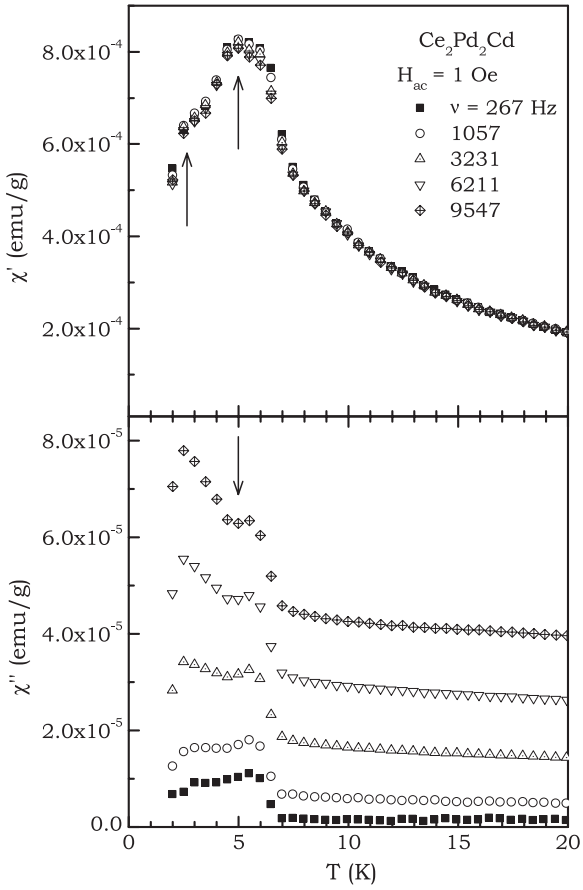

Figure 8. The real and imaginary parts of linear susceptibility (χ_1) for Ce_2Pd_2Cd measured in an ac field of 1 Oe and different frequencies. The anomalies observed are indicated by arrows.

compound CeCd has CsCl structure and orders ferromagnetically around 12 K [22–25]. Even although the compound is single phase up to the level of x-ray detection, we cannot rule out the possibility of the presence of a small CeCd impurity. With increasing field, the anomaly around 10 K diminishes and the peak around 5 K arises.

We now focus on the magnetic behaviour of Nd_2Pd_2Cd. In figure 4, we have shown $\chi(T)$ measured under $H = 10$ kOe. The χ remains flat with respect to temperature, with a small moment value in the temperature range 100–300 K, and then increases sharply below 50 K with a tendency to saturate below 5 K. From $d\chi/dT$ (inset in figure 4) we have precisely determined the Curie temperature (T_C) of Nd_2Pd_2Cd to be 23.7 K. Curie–Weiss behaviour is observed in the 100–300 K temperature range. The values of θ_p and μ_{eff}, determined from this linear region of χ^{-1} are 20.8(2) K and 3.49(3) μ_B/Nd mol respectively. Positive θ_p establishes the ferromagnetic interactions in this compound and the value of μ_{eff} establishes the trivalent state of neodymium. The experimental moment is close to the free ion value of 3.62 μ_B for Nd^{3+}.

We have also measured the susceptibility of Nd_2Pd_2Cd at different applied fields in order to ascertain the field induced magnetism in the ordered state. In figure 5 we have plotted the $\chi(T)$ measured at $H = 0.1$, 1 and 10 kOe under ZFC conditions. The plot also shows the FC measurements for $H = 1$ kOe. The upturn observed in $H = 10$ kOe is also observed at lower

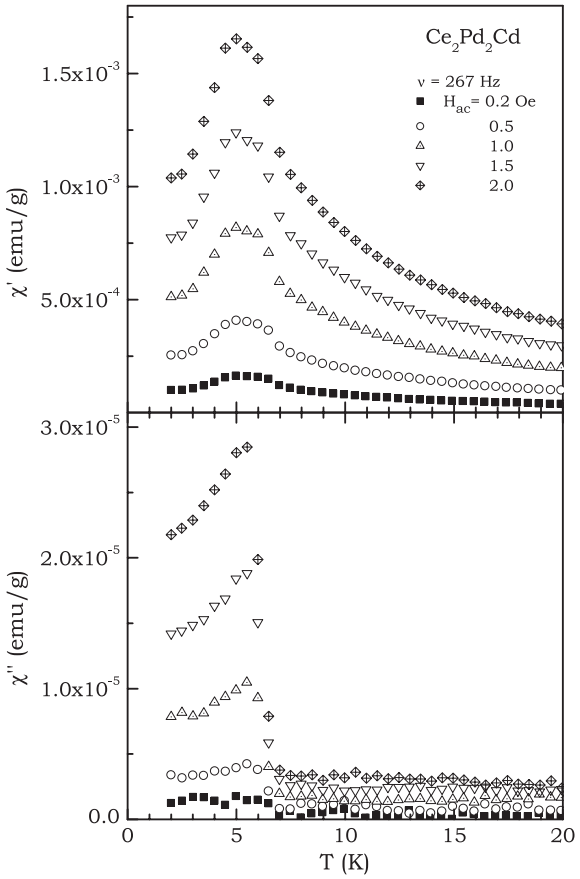

Figure 9. The real and imaginary parts of linear susceptibility (χ_1) for Ce_2Pd_2Cd measured at several ac fields and 267 Hz.

fields, indicating the presence of ferromagnetic ordering around 24 K. In the measurement at $H = 1$ kOe, the χ undergoes an upturn around 25 K, increasing rapidly with a tendency to saturate at low temperatures in both ZFC and FC states. However, the ZFC–FC bifurcates below 20 K, indicating the presence of spin-glass anomalies accompanying the ferromagnetic ordering.

3.3. dc magnetization

The magnetization, $M(H)$ curves for Ce_2Pd_2Cd measured up to 80 kOe are shown in figure 6. The magnetization measured at 2 K shows hysteretic behaviour where the loop broadens between 10 and 80 kOe. It is worth noting the observation of several steps in both up (increasing field) and down (decreasing field) cycles. In the up cycle, steps (indicated by vertical arrows) can be seen at high fields, between 40 and 80 kOe with a clear step around 70 kOe. In the down cycle however, steps can be more clearly seen at lower fields around 20 and 10 kOe. Such behaviour appears similar to that observed in Er_2Ni_2Pb [10]. In the inset of the $M(H)$ plots we have also plotted the first derivative of the $M(H)$, $\mathrm{d}M/\mathrm{d}H$ as a function of the field, to determine the fields at which the anomalies (steps) occur. The peaks in the plot of $\mathrm{d}M/\mathrm{d}H$

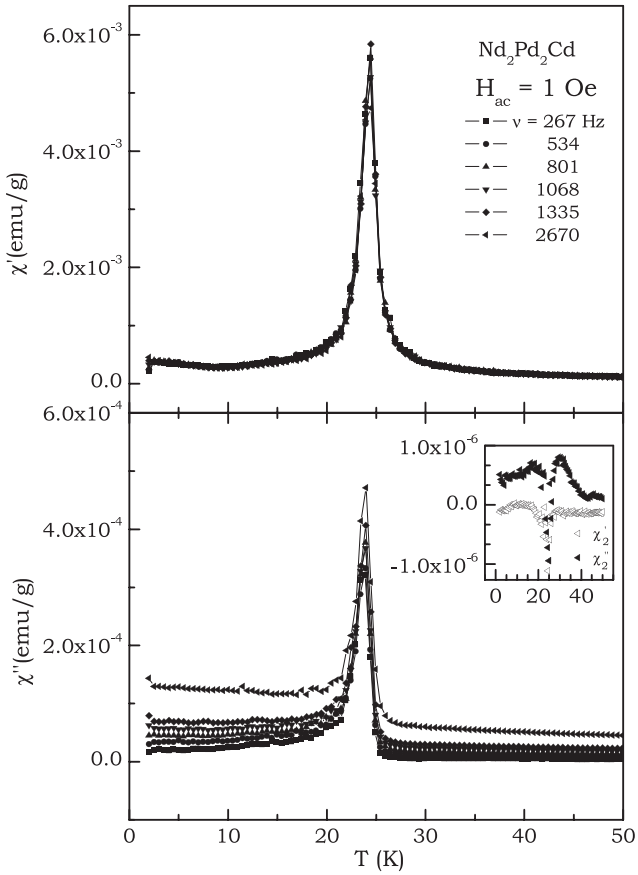

Figure 10. The real and imaginary parts of linear susceptibility (χ_1) for Nd_2Pd_2Cd measured in an ac field of 1 Oe and different frequencies. In the inset the real and imaginary part of the second harmonic component for $\nu = 2670$ Hz and $H_{ac} = 1$ Oe are shown to confirm the presence of ferromagnetic moment.

indicate the field induced magnetic transitions at 2 K. The $M(H)$ at 2 K reaches a value of about $1.7\mu_B$/Ce mol at 80 kOe, which is less than that expected for fully ordered Ce^{3+} ($g \times J = 2.14\ \mu_B$/Ce mol) but is in close agreement to other isostructural compounds such as Ce_2Pd_2In [7] and Ce_2Au_2Cd [15]. $M(H)$ at 2 K indicates closely spaced magnetic structures which are influenced by rapidly changing field. The magnetization at 5 K appears like that of an antiferromagnet, but is also hysteretic in the intermediate fields and does not saturate, but however reaches a slightly higher value at 80 kOe, indicating differences in the magnetism at these two temperatures. The steps seen at 2 K are missing here. $M(H)$ at 10 K is somewhat similar to that of 5 K in features, but is less hysteretic and has a smaller moment at 80 kOe. $M(H)$ measured at higher temperature, 20 K, increases linearly with applied field up to 40 kOe and then deviates marginally. There is a small gap in the up and down cycles for the fields between 20 and 70 kOe. The $M(H)$ of Ce_2Pd_2Cd establishes that the magnetic correlation persists up to a temperature as high as 20 K. At 20 K there is no hysteresis up to ± 5 kOe.

In figure 7 we show the magnetization of Nd_2Pd_2Cd measured at several temperatures spanning T_C. For all temperatures below 20 K, M initially increases rapidly for a small change

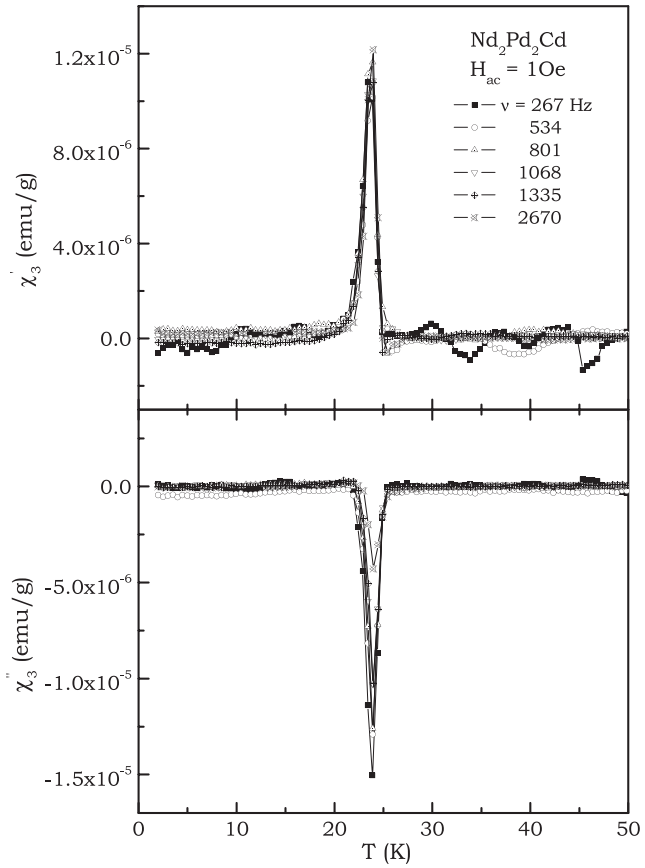

Figure 11. The real and imaginary parts of the non-linear susceptibility (χ_3) for Nd_2Pd_2Cd measured in an ac field of 1 Oe and different frequencies.

in H and varies slightly at higher fields as if saturating above 80 kOe. The saturation moment for Nd_2Pd_2Cd at 2 K/80 kOe is about $2\mu_B$/Nd mol, smaller than the possible value of 3.27 μ_B/Nd according to $g \times J$. The 2 K $M(H)$ curve is hysteretic at lower fields, although this is also observed at 5 and 10 K, but the width of the loop decreases with temperature. The features and moment values for $T = 2$, 5 and 10 K are similar. However, for $M(H)$ at 20 K, still in the magnetically ordered state, the feature is different. The initial rise in M for a small change in H has come down drastically at 20 K, still the value of saturation moment at 80 kOe is comparable with the lower temperature values. $M(H)$ at 50 K varies linearly with increasing field as expected in the paramagnetic state.

The $M(H)$ features of Nd_2Pd_2Cd in the ordered state do not fully comply with that of a ferromagnet, and hence in order to resolve this issue, we have also measured the hysteresis loops at all the temperatures at which $M(H)$ was measured. The hysteresis loops are shown as insets in the plots of $M(H)$ in figure 7. The well defined S-shape of the $M(H)$ loops accompanied by small hysteresis confirms the presence of spin-glass anomalies in this compound at low temperatures [28, 29]. The $M(H)$ loop at 50 K is again in agreement with the paramagnetic state, as if the spin-glass state coexists with ferromagnetism in the ordered state only.

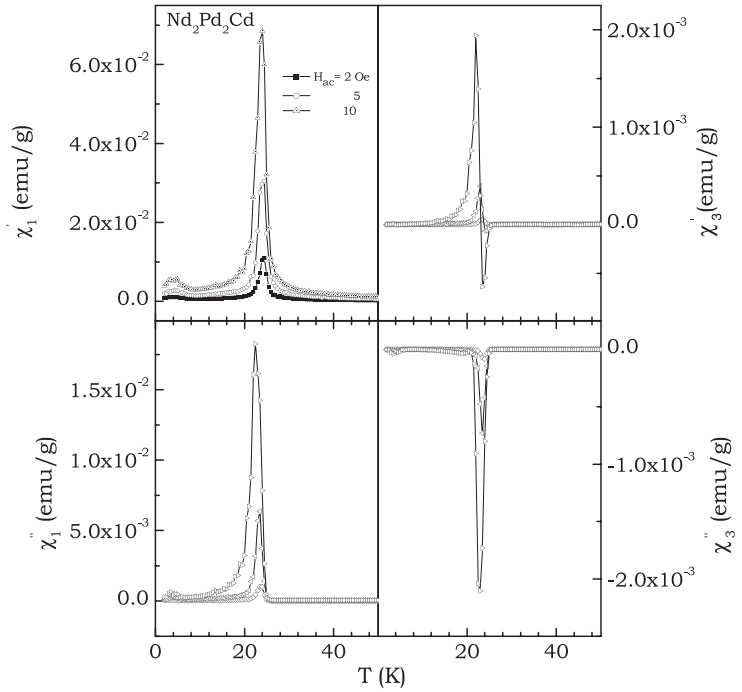

Figure 12. The real and imaginary parts of the linear (χ_1) and non-linear susceptibility (χ_3) for Nd_2Pd_2Cd measured at several ac fields and 267 Hz.

3.4. ac susceptibility

ac susceptibility studies, using the linear (χ_1) and non-linear susceptibilities (at 2nd or higher harmonics, e.g., χ_2, χ_3 and so on) have proven to be an important tool in studying the magnetic transitions from paramagnetic (PM)–ferromagnetic (FM) states [30–38]. The study of χ_3 is more useful in understanding the coexistence of ferromagnetism and spin-glass anomalies [30, 35, 37].

We have carried out ac susceptibility measurements on Ce_2Pd_2Cd at various frequencies up to the 3rd harmonics. In figure 8 we show the real and imaginary parts of the linear susceptibility (χ_1) measured under an ac field of 1 Oe. Consistent with the observation of a peak around 5 K in dc χ measurements, the real part of ac susceptibility (χ') exhibits a broad peak around 5 K, and there is no frequency dependence. There is also a small anomaly around 3 K. The imaginary part (χ'') exhibits a broad feature around 5 K and also a small anomaly around 3 K, which starts appearing prominently for higher frequencies ($\nu > 3$ kHz). In the non-linear susceptibility, i.e., ac susceptibility measured up to 3rd harmonics we could not detect any features expected for a compound with ferromagnetic interactions or spin-glass anomalies (and hence not shown here). In figure 9 we have plotted the ac χ measured at different amplitudes (0.2–2 Oe) and 267 Hz. The ac χ exhibits a broad peak at all the fields measured in the real and imaginary parts of the linear susceptibility. No features were observed at higher harmonics.

In comparison to Ce_2Pd_2Cd, the ac χ of Nd_2Pd_2Cd is quite interesting. In figure 10 we have shown the real and imaginary parts of the linear susceptibility (χ_1) measured under an ac field of 1 Oe. In the real part (χ'), the sharp peak observed at 25 K indicates the ordering

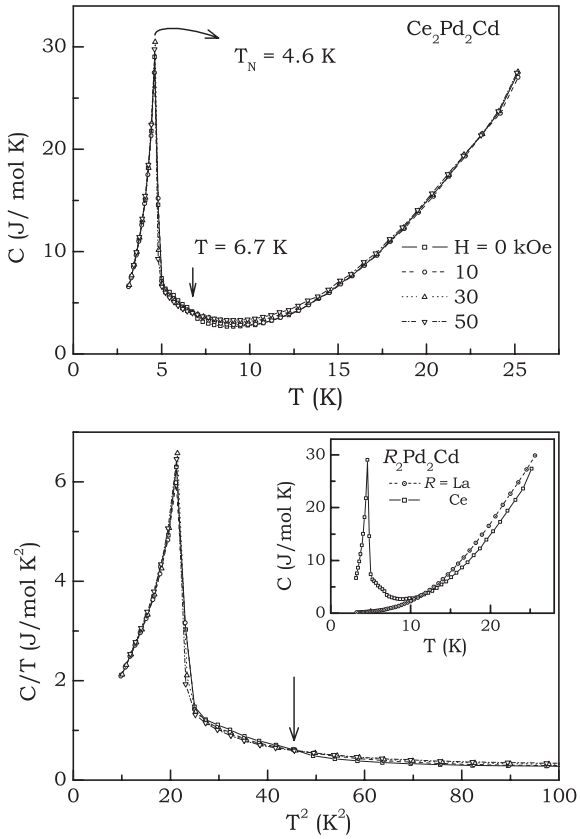

Figure 13. Specific heat for Ce_2Pd_2Cd measured in $H = 0$, 10, 30 and 50 kOe plotted in different ways. In the inset $C(T)_{H=0}$ is plotted for Ce_2Pd_2Cd and La_2Pd_2Cd to show the cross over of curves as described in the text.

temperature which is also observed in dc χ measurement. There is no frequency dependence, indicating long-range ordering at this temperature. The imaginary part of the ac susceptibility (χ'') also exhibits a sharp peak around 25 K and the features below this temperature are similar to the 're-entrant' spin glass systems, in which ferromagnetism coexists with spin-glass anomalies. It should be noted here that the signal in χ_2 is observed only if there is spontaneous magnetization. In order to ascertain the presence of a ferromagnetic moment, we have shown the signal observed at 25 K in χ_2 (both real and imaginary parts) as an inset in figure 10. The existence of a re-entrant spin-glass-like anomaly is further confirmed by the features of the imaginary part of χ_1 and the real part of χ_3 [30, 36]. We have plotted χ_3 (real and imaginary parts) measured at several frequencies under 1 Oe ac field in figure 11. The features of χ_3 taken together with the dc susceptibility measurements confirm the coexistence of ferromagnetism and spin-glass anomalies in Nd_2Pd_2Cd.

Figure 12 shows the real and imaginary parts of χ_1 and χ_3 measured at a frequency of 267 Hz and different ac amplitudes. At all the amplitudes, and in both forms of susceptibility, a definite sharp peak is seen around 25 K consistent with the ac and dc susceptibilities discussed above. The peak broadens at higher amplitudes indicating field induced changes in the magnetism of this compound.

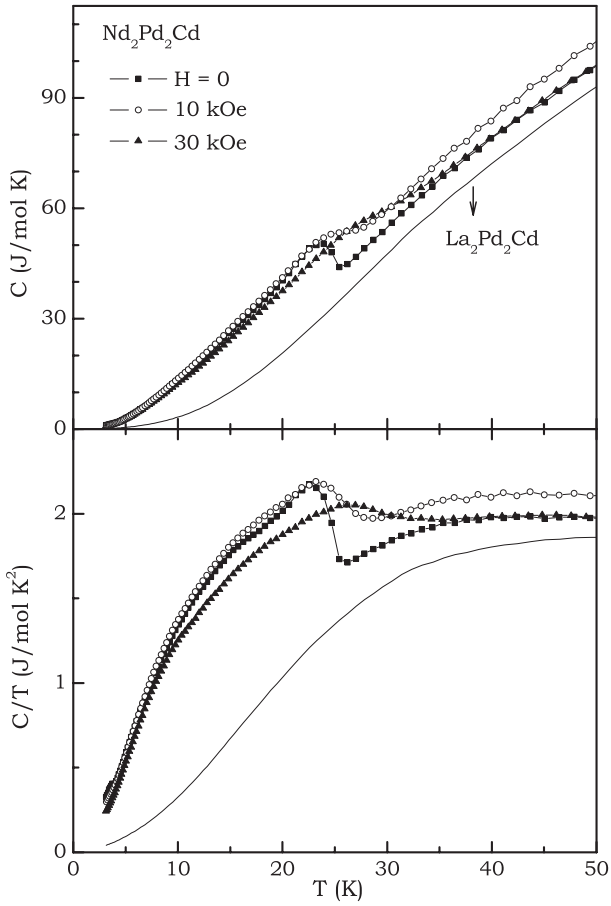

Figure 14. Specific heat of Nd_2Pd_2Cd measured in $H = 0$, 10 and 30 kOe plotted in several ways. The $C(T)$ for La_2Pd_2Cd is also plotted to show the non-magnetic reference for lattice subtraction. See the text for details.

3.5. Heat-capacity measurements

We have measured specific heat for Ce_2Pd_2Cd in the temperature range of 3–25 K using a pre-calibrated heat capacity puck. In figure 13 we have plotted the specific heat (C) in different ways. $C(T)$ for Ce_2Pd_2Cd in zero field reaches a minimum below 10 K, and then rises sharply at 5 K exhibiting a sharp peak at 4.6 K. $C(T)$ then falls sharply at lower temperatures. The non-T^3 behaviour of $C(T)$ is clearly seen in the plot of C/T versus T^2, plotted in the bottom panel of figure 13. The continuous change in C at lower T indicates the presence of another magnetic state below 3 K. We have also measured $C(T)$ for Ce_2Pd_2Cd under applied fields of 10, 30 and 50 kOe. As can be seen clearly from figure 13, there is no effect of the external magnetic field on the features of the heat capacity. Measurements done at these fields show the features, explained above for $H = 0$. $C(T)_H$ curves also reach minima below 10 K before undergoing the antiferromagnetic ordering. Such phenomena are usually associated with the Kondo effect. It is interesting to note here that curves of $C(T)$ measured under different fields cross each other at 6.7 K. The crossing of heat capacity curves measured at different fields have

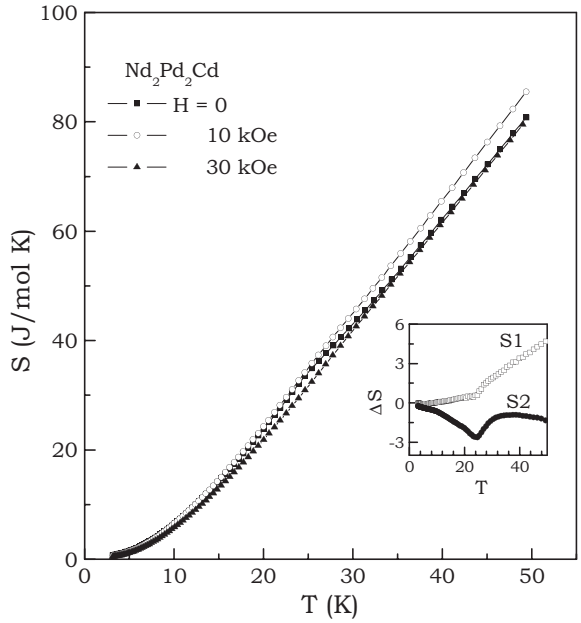

Figure 15. Total entropy (S) for Nd_2Pd_2Cd in $H = 0$, 10 and 30 kOe. The inset shows the change in entropy when field is changed. The curve S1 indicates change of field from 0 to 10 kOe and S2, 0 to 30 kOe.

been attributed to heavy fermion behaviour, and has been observed in Ce_2Au_2Cd and Ce_2Au_2In also [15, 26, 27].

Now we turn our attention to the heat capacity of ferromagnetically ordering Nd_2Pd_2Cd. Figure 14 shows C and C/T versus T for Nd_2Pd_2Cd measured in zero and applied fields. $C(T)$ measured in zero applied field shows a well defined λ anomaly around 24 K, as the system undergoes long-range ordering. The application of a 10 kOe field marginally affects the peak shape, but it is still clearly seen (see C/T versus T in the bottom panel). The peak appears to be marginally shifted to a higher temperature. Increasing field strength to 30 kOe completely smears out the well defined peak and pushes it further to higher temperature. From the linear region of C/T versus T^2 (in the range of 3–5 K), we have estimated the values of γ (table 4) and used it to calculate the total entropy (S, J mol^{-1} K^{-1}) of the system in zero and applied fields. The plot of total entropy for Nd_2Pd_2Cd in $H = 0$, 10 and 30 kOe is shown in figure 15. $S(T)$ for $H = 0$ undergoes a change around 24 K as if the entropy is released at this temperature. The change in $S(T)$ with the application of field (i.e. changing the field from 0 to 10 kOe, marked as S1 and 0 to 30 kOe, S2) is shown as an inset of figure 15. The value of ΔS for S2 at 24 K is about 3 J mol^{-1} K^{-1} (around 43 mJ K^{-1} cm^{-3}), which implies that Nd_2Pd_2Cd is a candidate qualifying as a 'magnetocaloric' compound [39]. It is interesting to observe the sign reversal between S1 and S2. It has been shown that for ferromagnets, the sign of ΔS is negative (as seen in S2). But for S1, there is a very small effect of the field on the entropy and it remains positive throughout the temperature regime.

In order to determine the magnetic contribution to the heat capacity (C_{mag}) of Nd_2Pd_2Cd, we have subtracted the lattice part using the heat capacity of La_2Pd_2Cd (shown in figure 14) as a reference and assumed that the lattice and electronic contributions originating from phonon excitations and conduction electrons respectively, are similar in both isostructural compounds.

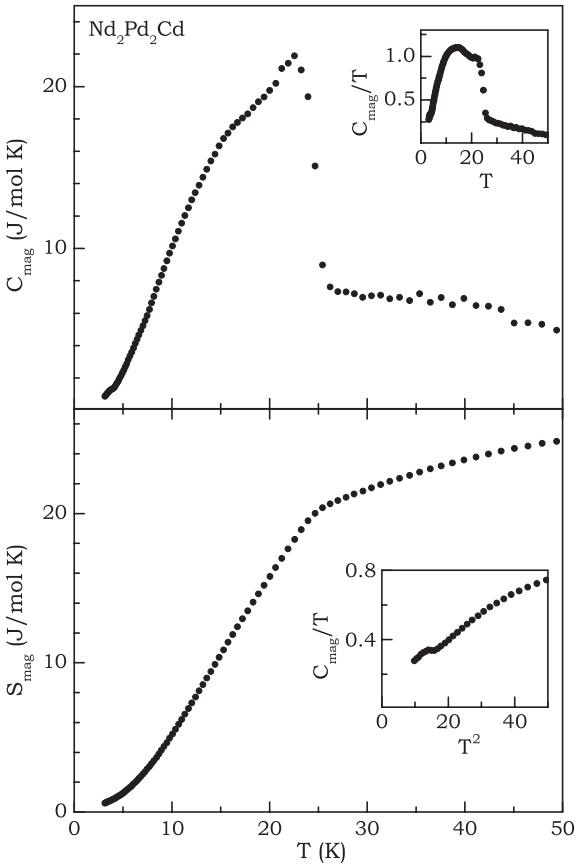

Figure 16. Magnetic part of heat capacity (C_{mag}) and entropy (S_{mag}) for Nd_2Pd_2Cd, obtained by subtracting the lattice part $C_{La}(T)$. C_{mag} is plotted in different ways in the two insets.

Table 4. Values of electronic coefficient of heat capacity (γ), the lattice contribution (β) and Debye temperature (Θ_D) calculated from heat capacity measurements on Nd_2Pd_2Cd at various applied fields. The values shown in parenthesis are the errors in calculation.

H (kOe)	γ (mJ mol^{-1} K^{-2})	β (mJ mol^{-1} K^{-4})	Θ_D (K)
0	131(±11)	20(±1)	46(±1)
10	135(±5)	17(±1)	49(±1)
30	57(±5)	19(±1)	47(±1)

In figure 16 we have shown C_{mag} and the magnetic entropy, S_{mag}. There is a sharp peak in the plot of C_{mag} versus T corresponding to the ferromagnetic ordering around 24 K. However there is a broad anomaly around 15 K (more clearly seen in C_{mag}/T versus T also) with a small jump in C_{mag} around 5 K. The origin of this anomaly is unknown at present. We anticipate that this anomaly can be substantiated with the anomalies observed for Nd_2Pd_2Cd at low temperatures in the magnetic measurements. We used the lowest temperature linear region in the plot of C_{mag}/T versus T^2 (3–5 K) to calculate the γ (electronic coefficient of

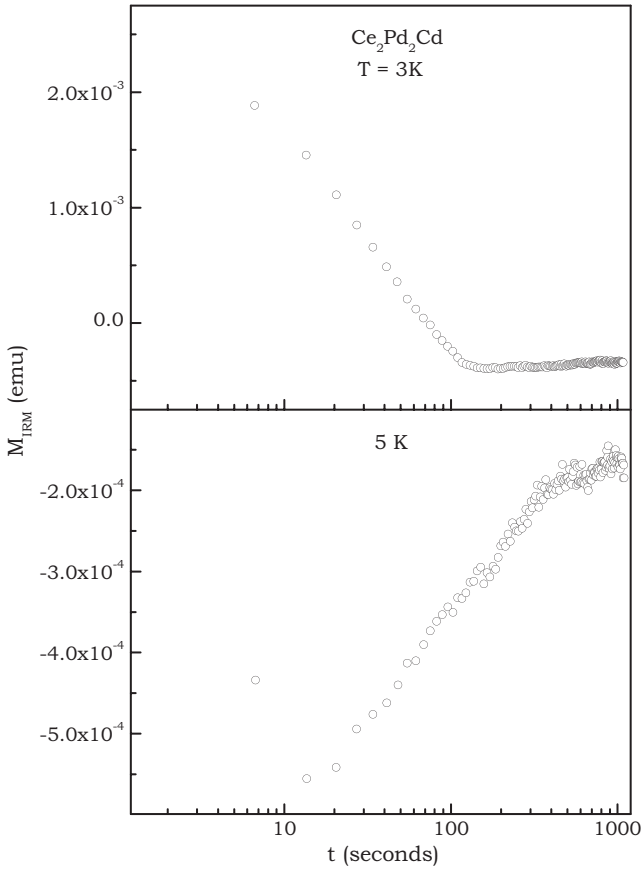

Figure 17. Relaxation behaviour of spins for Ce_2Pd_2Cd at $T = 3$ and 5 K. Time (seconds) is shown on a log scale.

heat capacity), β (coefficient of lattice contribution) and Θ_D (Debye temperature), which are 115(2) mJ mol^{-1} K^{-2}, 16(2) mJ mol^{-1} K^{-4} and 49(1) K respectively. The plot of $S_{mag}(T)$ undergoes a drastic change around 24 K and tries to saturate above T_C.

3.6. Isothermal remanent magnetization (relaxation) measurements (M_{IRM})

In figures 17 and 18 we have shown the relaxation behaviour of Ce_2Pd_2Cd and Nd_2Pd_2Cd, respectively. The M_{IRM} was measured for both compounds by cooling the sample to the measurement temperature in zero field and then applying a field of 5 kOe for 5 min after the temperature is stabilized. The field was switched off and M_{IRM} was measured over a definite period of time as soon as the field reached zero. For the cerium compound M_{IRM} was measured at 3 and 5 K (figure 17). At 3 K, M_{IRM} relaxes quickly within a few seconds to the lowest value and then levels off, however, at 5 K, still in the vicinity of the ordering temperature, there is a very rapid quenching of M_{IRM} as soon as the field is removed and there is practically no relaxation. In figure 18, we have shown the M_{IRM} of the neodymium compound measured at 5, 10 and 20 K (all below the ordering temperature). Similarly to the cerium compound, the neodymium compound also does not show any logarithmic relaxation behaviour, even at the

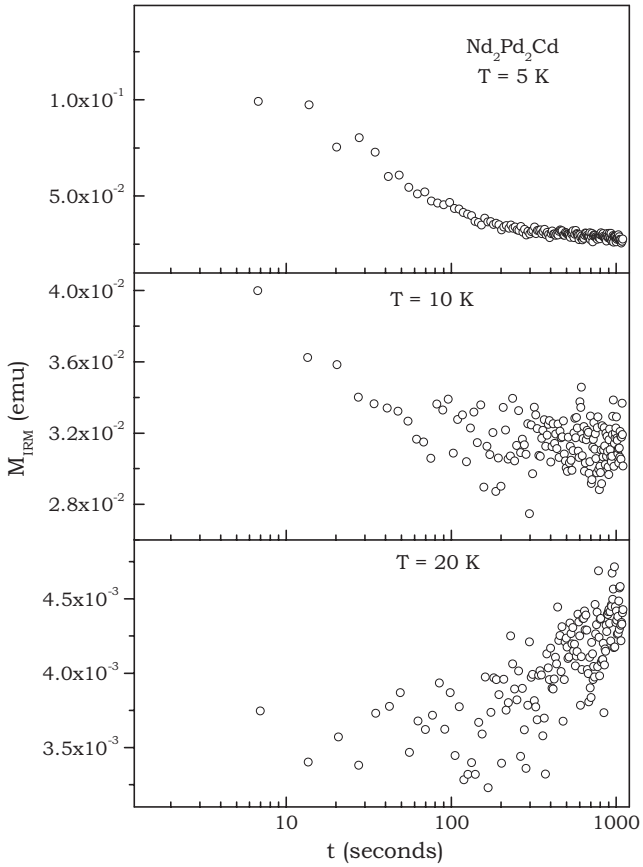

Figure 18. Relaxation behaviour of spins for Nd_2Pd_2Cd at $T = 5$, 10 and 20 K. Time (seconds) is shown on a log scale.

lowest temperature. At 5 K, M_{IRM} relaxes non-logarithmically and levels off after more than two decades of time. There is very weak relaxation at 10 K and no relaxation at 20 K.

4. Conclusions

We have synthesized and structurally characterized the series of isostructural RE_2Pd_2Cd compounds with RE = La, Ce and Nd and carried out detailed investigations of their physical properties. The magnetic and specific heat measurements of Ce_2Pd_2Cd suggest that it is a heavy fermion compound with Kondo interactions. Nd_2Pd_2Cd undergoes ferromagnetic ordering and exhibits spin-glass anomalies at low temperatures. Detailed neutron scattering experiments are required to understand the true nature of magnetic ordering in these compounds and can be quite rewarding in understanding the structure–property relations.

Acknowledgments

This work was supported by the Deutsche Forschungsgemeinschaft. SR is indebted to the Alexander von Humboldt Foundation for a postdoc stipend.

References

[1] Lukachuk M and Pöttgen R 2003 *Z. Kristallogr.* **218** 767
[2] Pöttgen R, Fugmann A, Hoffmann R-D, Rodewald U Ch and Niepmann D 2000 *Z. Naturf.* b **55** 155
[3] Hulliger F and Xue B Z 1994 *J. Alloys Compounds* **215** 267
[4] Giovannini M, Michor H, Bauer E, Hilscher G, Rogl P and Ferro R 1998 *J. Alloys Compounds* **280** 26
[5] Giovannini M, Michor H, Bauer E, Hilscher G, Rogl P, Bonelli T, Fauth F, Fischer P, Herrmansdörfer T, Keller L, Sikora W, Saccone A and Ferro R 2000 *Phys. Rev.* B **61** 4044
[6] Ijiri Y and DiSalvo F J 1996 *J. Alloys Compounds* **233** 69
[7] Kaczorowski D, Rogl P and Hiebl K 1996 *Phys. Rev.* B **54** 9891
[8] Hauser R, Michor H, Bauer E, Hilscher G and Kaczorowski D 1997 *Physica* B **230–232** 211
[9] Chinchure A D, Sandoval E M and Mydosh J A 2002 *Phys. Rev.* B **66** 20409R
[10] Chinchure A D, Sandoval E M and Mydosh J A 2001 *Phys. Rev.* B **64** 20404R
[11] Strydom A M 2005 *J. Alloys Compounds* **394** 152
[12] Niepmann D, Pöttgen R, Künnen B and Kotzyba G 2000 *J. Solid State Chem.* **150** 134
[13] Stadler F, Fickenscher Th and Pöttgen R 2001 *Z. Naturf.* b **56** 1241
[14] Mishra R, Pöttgen R, Hoffmann R-D, Kaczorowski D, Piotrowski H, Meyer P, Rosenhahn C and Mosel B D 2001 *Z. Anorg. Allg. Chem.* **627** 1283
[15] Rayaprol S and Pöttgen R 2005 *Phys. Rev.* B **72** 214435
[16] Rayaprol S and Pöttgen R 2006 *Phys. Rev.* B at press
[17] Canepa F, Cirafici S, Merlo F, Pani M and Ferdeghini C 1999 *J. Magn. Magn. Mater.* **195** 646
[18] Pöttgen R, Gulden Th and Simon A 1999 *GIT Labor-Fachz.* **43** 133
[19] Kußmann D, Hoffmann R-D and Pöttgen R 1998 *Z. Anorg. Allg. Chem.* **624** 1727
[20] Yvon K, Jeitschko W and Parthé E 1977 *J. Appl. Crystallogr.* **10** 73
[21] Sheldrick G M 1997 *SHELXL-97, Program for Crystal Structure Refinement* University of Göttingen
[22] Olcese L 1963 *Atti. Acad. Naz. Lincei. Rend. Sci. Fiz. Mat. Nat.* **35** 7
[23] Buschow K H J 1974 *J. Chem. Phys.* **61** 4666
[24] Alfieri G T, Banks E, Kanematsu K and Ohoyama T 1967 *J. Phys. Soc. Japan* **23** 507
[25] Buschow K H J 1979 *Rep. Prog. Phys.* **42** 1373
[26] Vollhardt D 1997 *Phys. Rev. Lett.* **78** 1307
[27] Mock S, Faisst A and Löhneysen H v 1997 *Phys. Rev.* B **56** 335
[28] Binder K and Young A P 1986 *Rev. Mod. Phys.* **58** 801
[29] Prejean J J and Souletie J 1980 *J. Physique* **41** 1335
[30] Chakravarti A, Ranganathan R and Bansal C 1992 *Solid State Commun.* **82** 591
[31] Suzuki M 1977 *Prog. Theor. Phys.* **58** 1151
[32] Taniguchi T, Miyako Y and Tholence J L 1985 *J. Phys. Soc. Japan* **54** 220
[33] Coles B R 1984 *Phil. Mag.* B **49** L21
[34] Kunkel H P and Williams G 1988 *J. Magn. Magn. Mater.* **75** 98
[35] Chakravarti A, Ranganathan R and Roy S B 1992 *Phys. Rev.* B **46** 6236
[36] Nair S and Banerjee A 2003 *Phys. Rev.* B **68** 94408
[37] Mukherjee S, Ranganathan R, Chakravarti A and Sil S 2001 *J. Magn. Magn. Mater.* **224** 210
[38] Tsurkan V, Hemberger J, Klemm M, Klimm S, Loidl A, Horn S and Tidecks R 2001 *J. Appl. Phys.* **90** 4639
[39] Gschneidner K A Jr and Pecharsky V K 2000 *Annu. Rev. Mater. Sci.* **30** 387
Gschneidner K A Jr, Pecharsky V K and Tsokol A O 2005 *Rep. Prog. Phys.* **68** 1475